MODEL-BASED METHOD FOR IMPROVING THE ACCURACY AND REPEATABILITY OF ESTIMATING VASCULAR BIFURCATIONS AND CROSSOVERS FROM RETINAL FUNDUS IMAGES

Chia-Ling Tsai[1], Charles V. Stewart[1], Howard L. Tanenbaum[2], and Badrinath Roysam[1]

[1]Rensselaer Polytechnic Institute, Troy, New York 12180.

[2]The Center for Sight, 349 Northern Blvd., Albany, NY 12204.

ABSTRACT

A model-based algorithm, termed exclusion region and position refinement (ERPR), is presented for improving the accuracy and repeatability of estimating the locations where vascular structures branch and cross over, in the context of human retinal images. The goal is two fold. First, accurate morphometry of branching and crossover points (landmarks) in neuronal/vascular structure is important to several areas of biology and medicine. Second, these points are valuable as landmarks for image registration, so improved accuracy and repeatability in estimating their locations and signatures leads to more reliable image registration for applications such as change detection and mosaicing. The ERPR algorithm is shown to reduce the median location error from 2.04 pixels down to 1.1 pixels, while improving the median spread (a measure of repeatability) from 2.09 pixels down to 1.05 pixels. Errors in estimating vessel orientations were similarly reduced from 7.2 degrees down to 3.8 degrees.

Index Terms: Biomedical Image Analysis, Retinal Images, Landmarks, Bifurcations, Crossovers, Feature Extraction, Feature Stability, Feature Refinement, Image Registration, and Mosaic Synthesis.

Correspondence:
Prof. Badrinath Roysam,
Rm JEC 6046, ECSE Department,
Rensselaer Polytechnic Institute,
Troy, New York 12180-3590, USA.
Phone: 518-276-8067,
Fax: 518-276-6261,
Email: roysam@ecse.rpi.edu

I. Introduction

The quantitative analysis of branched structures such as neurons and vasculature is important to biology and medicine [1, 2, 3, 4, 5, 6, 7, 8, 9]. Branching and crossover points of vascular structures are of special interest [10, 11, 12, 2, 13]. One such application is the early diagnosis of hypertension by measuring changes in select vascular branching and crossover regions [14, 15]. These points are also important from a purely image analysis standpoint. If stable, they are valuable as features (i.e., landmarks) for registration, mosaicing, and change detection. The pattern of intersection angles and vessel thickness can be used as landmark signatures [13, 16]. Fig. 2 illustrates instances of landmark-based registration and mosaicing. In this work, the branching and crossover points are used for registration. Accurate and repeatable landmarks are crucial to registration performance. Landmark repeatability plays three crucial roles - reducing the number of possible correspondences between two images; accurately initializing a local transformation for registration; and minimizing the feature extraction computation since better initialization improves the likelihood of successful registration [13, 17].

In prior work, we have described fast and robust model-based algorithms for tracing the retinal vasculature in an exploratory manner [4, 7]. The model underlying these algorithms expects a fragment of the vasculature to consist of two relatively straight, anti-parallel edges with either an intensity peak or an intensity valley in between.

The present paper extends our prior work by greatly improving the accuracy and repeatability with which branching and crossover points are extracted. It is based on the observation that while the "anti-parallel edges" model is an excellent basis for tracing the linear portions of the vasculature, it is not an adequate basis for describing the branching and crossing points. Indeed, these are locations where the model breaks down, introducing errors in the estimated landmark coordinates, and consequently the angles as well. This phenomenon is illustrated in Fig. 2.

II. Background to the Present Study – Exploratory Tracing Algorithms

The exploratory approach to vessel tracing (see Fig. 1, and [4]) is based on a localized anti-parallel edge pair model. It proceeds in three stages.

Step 1 (seed point initialization): The algorithm analyzes the image along a coarse grid (see Fig. 1(b) to gather gray-scale statistics (contrast and brightness levels) and to detect seed locations on vessels -- gray-scale minima between opposite signed 1-D edges.

Step 2 (recursive tracing): The second stage, illustrated in Fig. 1(a) is a sequence of recursive tracing steps that are initiated at each of the filtered seed points, and proceed along vessel centerlines assuming an anti-parallel edge model.

Step 3 (landmark extraction): The tracing that starts from a seed point continues until the end of the vessel is reached or until the centerline of the tracing intersects a previously detected vessel centerline. Landmarks are placed at intersections of traces and at locations where three or more centerline traces (see Fig. 1(b)) meet. These landmarks are characterized by this location and by the orientations of the traces meeting to form the landmark. Example traces and landmarks are shown in Fig. 1(b).

III. Limitations of Prior Methods

Landmark extraction in the exploratory tracing algorithm above is conceptually simple, and effective in terms of detection. However, it suffers from two limitations relating to the accuracy and repeatability of estimating the intersection coordinates and angles.

These limitations arise primarily from the fact that the anti-parallel edge model on which the tracing algorithm is based, is no longer valid very close to branching and crossover points due to the rounded nature of the junctions (see Fig. 3). Consequently, when the recursive tracing steps (equation (1)) approach a junction, the estimation of the centerline of the vessels is less accurate. This may result in uncertain, even apparently random placement of centerline points (Figs. 2 & 4) occasionally.

This estimation is also influenced by variations in the locations of the seed points, implying that the *repeatability* with which the centerline is estimated is impaired as well. Finally, errors in estimating the point of intersection have a pronounced effect on the accuracy with which the intersection angles are estimated. The issues related to landmark accuracy are illustrated in Fig. 2. The issues related to repeatability are illustrated in Fig. 4.

IV. Exclusion Region and Position Refinement (ERPR) Method

4.1 A Model for Intersections

As noted above, failure of the anti-parallel edges model near intersections is the primary source of error. To address this, we introduce an explicit model of the structure of a landmark and an estimation technique that estimates the parameters of this model. The proposed landmark model, illustrated in Fig. 3, consists of three parts:

1. A circular exclusion region: This region models the region of intersection of the vessels. In this region, the anti-parallel model of the vessels is violated. Therefore, traces computed in this region are not used.

2. The landmark location: This is defined as the (x, y) point nearest the extrapolation of the centerlines of the vessels that meet to form the landmark in the least-squares sense.

3. Orientation vectors: The set of vessel orientations that meet to form the intersection, defined relative to the landmark location.

The exclusion region radius is estimated once, but the other parameters -- the landmark location and the vessel orientations -- are estimated iteratively. The following sub-sections provide a more detailed description.

4.2 Algorithm Overview

The starting point for the estimation is the endpoint of a trace when either it intersects the boundary of another vessel or it meets at least two other trace endpoints. From this endpoint, the algorithm gathers information about neighboring traces, estimates the initial landmark point, determines the exclusion radius, and estimates the initial vessel orientations. This initializes an iterative process that alternates steps of re-estimating traces and orientations of vessels outside the exclusion region, and then re-estimating the landmark point from the vessels.

4.3 Gathering Information About Neighboring Traces

The estimation technique for a single landmark starts from a trace endpoint and a set of neighboring traces. Fig. 3 illustrates the terminology and notation. A *trace* is defined as a sequence of centerline points detected during recursive tracing starting from a single seed point. Let T be the set of all traces (across the entire image), $t \in T$ be a single trace, and

$P(t) = [p_{t,0}, p_{t,1}, \ldots p_{t,i} \ldots]$ be the sequence of centerline points on trace *t*. The centerline points on trace *t* are denoted $p_{t,i}$. The ending point of the trace is denoted $p_{t,e}$. The set of neighboring traces, denoted by $N(p_{t,e})$, is the set of traces having at least one other centerline point close to endpoint $p_{t,e}$. Finally, let $w_{t,i} = w(p_{t,i})$ be the width of the vessel at each centerline point, computed easily during recursive tracing.

Following termination of tracing for a specific trace t^* and endpoint $p_{t^*,e}$ the set of neighbor traces, denoted $N(p_{t^*,e})$ is found. This set is defined as

$$N(p_{t^*,e}) = \left\{ t \in T \mid \min_{p \in P(t)} \left\| p_{t^*,e} - p \right\| \le w(p) \right\}. \quad (2)$$

In other words, the set $N(p_{t^*,e})$ contains all traces having at least one centerline point, p, closer to $p_{t^*,e}$ than the vessel width at p. The search for neighbor traces is expedited by storing trace points in regularly spaced, $n \times n$ bins covering the entire image.

The last step in the gathering process is to compute the set of closest points to $p_{t^*,e}$ from the traces in $N(p_{t^*,e})$. Indeed, this determines if a landmark should even exist. Denote this set as:

$$C(p_{t^*,e}) = \left\{ p \mid \min_{p \in P(t)} \left\| p_{t^*,e} - p \right\|, t \in N(p_{t^*,e}) \right\}. \quad (4)$$

4.4 Initializing the Landmark Model Parameters

During the initialization process, the landmark location, the exclusion region radius, and the vessel orientations are estimated. The exclusion region radius remains fixed throughout the computation.

Initializing the landmark location using $C(p_{t^*,e})$ only if $C(p_{t^*,e})$ contains at least three endpoints - the initial landmark location, denoted q^0, is the centroid of the endpoints.

The exclusion radius r^* is then estimated as the maximum of the trace widths for all traces in $N(p_{t^*,e})$. There is no need to refine r^* because it does not depend significantly on the landmark location or other landmark parameters.

The final step in initialization is estimating the vessel orientations near the intersection. This orientation is denoted $\theta(t)$ for each trace $t \in N(p_{t^*,e})$. The initial value of this orientation, $\theta^0(t)$,

is found by fitting a line to points on trace *t* that are just outside the exclusion region. This is described in more detail below because it is exactly the same computation as used in the iterative procedure.

4.5 Iterative Estimation of Model Parameters

The trace centerlines, vessel orientations, and landmark location are estimated iteratively. In the j^{th} iteration, the refined trace centerline locations and vessel orientations are $P^j(t)$ and $\theta^k(t)$ for $t \in N(p_{t^*,e})$. Note that $P^0(t)$ is the initial sequence of trace points. The landmark location in iteration *j* is q^j.

The first step in each iteration, i.e., for $j \geq 1$, is to re-estimate the trace centerline points near landmark location q^{j-1}, but outside the exclusion region. This procedure is called *back-trace refinement,* and is illustrated in Fig. 3. For each trace $t \in N(p_{t^*,e})$, a seed point on the boundary of the exclusion region is found, and then the recursive tracing procedure described in Section II is run for a small number of steps (e.g., *n* = 5) away from the intersection. The seed point is defined as the intersection point of a ray from the previous landmark location in the previous vessel direction and the boundary of the exclusion region. The refined trace points replace the corresponding trace points to form the set $P^j(t)$ from $P^{j-1}(t)$ at the j^{th} iteration.

The next step is to re-estimate the orientation of the vessel associated with each trace *t* from the trace points and landmark location. The *n* points in $P^j(t)$ closest to q^{j-1} but outside the exclusion region are found. These points are exactly the new trace points just computed. For each trace, these points are placed in a set *S* together with the previous landmark location, q^{j-1}, and the orthogonal least-squares regression line $L^j(t)$ is computed from this set. The previous landmark location is added to ensure stability, especially for intersections with acute angles. The new orientation is taken from the line parameters.

The final step is to estimate the new landmark location, q^j. This is computed from the line parameters $L^j(t)$ that have been just estimated. The specifics of doing this depend on the line representation, but are equivalent. For example, if $L^j(t)$ is represented by a unit normal $\hat{\eta}^j(t)$, and point $p^k(t)$ (any point on the line will do), then q^k is the point minimizing the least-squares

criterion $\sum_{t \in N(p_{t^*,e})} [\hat{\eta}^k(t) \cdot (p^k(t) - q^k)]^2$. This point is unique unless all lines are parallel, which of course cannot happen in this application. The iterative process terminates when the landmark location stabilizes -- specifically, $\| q^j - q^{j-1} \| < 0.25$ pixels -- or the number of iterations exceeds a limit.

4.6 Simplified Estimation of Landmark Model Parameters

The most expensive (and unstable) part of the estimation process is back-trace refinement. It makes sense to consider the possibility of a simpler algorithm where back-trace refinement is removed from the iterative estimation process and only applied at the end. This simplified process proceeds as follows: The lines $L^j(t)$ are estimated for each trace $t \in N(p_{t^*,e})$. Then, the refined landmark location q^j is estimated from these lines. After the iterative process, a single full iteration is applied, including back-trace refinement, line estimation, and landmark location estimation.

Using the same test criterion as above, if the new location is too far from the previous one, the landmark location is restored to its previous value. Intuitively, this should work because it should be possible to obtain a reasonably accurate estimate of the landmark location from the traces outside the exclusion region, and allowing final accuracy of the centerline positions, trace orientations, and then landmark position to be achieved in just a single full iteration.

V. Experimental Evaluation

Accuracy and repeatability of the proposed ERPR technique was evaluated on datasets from 18 different eyes, with 10-20 images in each data set. Each image is of size 1024×1024 pixels, and was captured using a Topcon IMAGENET digital camera system at the Center for Sight (Albany, New York). The evaluation method is based on a highly accurate registration algorithm based on a 12-parameter transformation model (see 16 for detailed description and error analysis). As noted below, its accuracy can be made independent of landmark location accuracy, so it can be used as a testbed and standard for measuring landmark estimation errors. The average alignment error of this algorithm, as measured by the distance between trace centerlines

is 0.83 pixels on 1024×1024 images. This algorithm models the retina as a curved quadratic surface that is imaged by a weak-perspective uncalibrated camera.

The last step of the registration algorithm noted above is especially significant. It uses a localized sum-of-squared-differences (SSD) technique [18] to correct the registration for errors in estimating landmark locations (based on the original tracing and landmark localization technique [4]). This step is computationally expensive, taking almost 90% of the total computation time, due to extensive pixel processing. The registration accuracy using the un-refined landmarks is 1.59 pixels, and using the SSD matching technique is 0.83 pixels. Indeed, these observations served as a motivation to explore alternative methods for estimation of landmark locations.

The ability to register retinal images with sub-pixel accuracy *in spite of errors in estimating the landmark locations (albeit at a high computational price)* leads to several methods of evaluating the proposed Exclusion Region and Position Refinement (ERPR) algorithm.

- **Repeatability Measurement:** For a landmark that appears in two or more images, registering the images places the two different estimated positions in the same coordinate system. This gives us a measure of the *repeatability* of the landmark position, modulo the transformation error itself.
- **Accuracy Measurement:** We can compare the SSD refined positions obtained just prior to convergence to the estimated landmark positions as a further measure of position *accuracy*.
- We can analyze the effect of the accuracy of landmark positions on the estimate of the quadratic transformation.
- We can generate a qualitative, visual indication of the effectiveness of the ERPR technique by transforming many different images of the same landmark into the same coordinate system. Examples are shown in Fig. 7.

The first quantitative measure is the error between corresponding landmarks in registered pairs of images. Let q_1 be the landmark location in image I_1 and q_2 be the landmark location in image I_2. Let $\Theta_{1,2}$ be the estimated registration function mapping I_1 onto I_2, so that $\Theta_{1,2}(q_1)$ is the mapping of the landmark location into image I_2. The local distance $\| \Theta_{1,2}(q_1) - q_2 \|$ gives one measure of the landmark error. The maximum difference in trace orientations between the

mapping of the landmark at q_1 and the landmark at q_2 gives a second measure. By combining these measures over all landmarks in all registered image pairs, we obtain summary statistics on the repeatability of the estimated landmark parameters.

Table 1 shows summary statistics for the original landmark detection technique and for several versions of the proposed ERPR technique, including the full method, the simplified method using just one iteration of back trace refinement, and a version where back trace refinement is not used at all. Clearly, the ERPR method is twice as repeatable as the original method, both in terms of position and orientation. In fact, it may be higher because of the inherent error in the transformation. Second, there is little difference between the fully iterative ERPR and the simplified version where back trace refinement is used only once. Third, with no use of back-trace refinement the results are substantially worse. Based on the latter two conclusions, the remaining experiments will focus exclusively on the ERPR with one step of back trace refinement.

The second quantitative comparison is between the SSD-refined landmark positions that emerge at the end of registration and the positions estimated by either the original landmark technique, or by ERPR. Using corresponding point locations q_1 and q_2, as above, the SSD step during estimation of $\Theta_{1,2}$ refines the position of q_2 to match the transformation of a small region surrounding q_1. Call the new position q'_2. The error measure is then $\| q_2 - q'_2 \|$. Interestingly, this measure is not sensitive to minor errors in the transformation, and therefore an even better measure of the repeatability of the landmark position estimate. *The disadvantage is that the SSD refinement gives no improvement in orientation accuracy.*

The results of this measure taken over all correctly registered pairs from our data set are shown in Table 2. Both median and average errors are given. The advantage of the new ERPR method with just a single iteration of back-trace refinement is striking. The average error is 2.5 times lower and the median error is 1.9 times lower.

The final quantitative analysis is to consider the effect of the new landmark model and estimation technique on the registration algorithm itself. The major question is whether or not the landmark positions are accuracy enough to eliminate the SSD-refinement step altogether. SSD-refinement step in fact consists of two steps: one is the landmark position refinement as discussed above, and the second is SSD-based matching of landmarks detected in one image but

missing in the other. The second step occurs after the first. To summarize, using the original landmark model and localization technique and no position refinement, the registration error is 1.59 pixels. Using the original landmark model, and the first step of SSD refinement, the registration error is 0.97 pixels. Using the original landmark model and both SSD refinement steps, the registration error is 0.83 pixels. Using the new landmark model, ERPR, with a single iteration of back trace refinement at each landmark and no SSD refinement, the error drops to 1.21. This is certainly a dramatic improvement but not as accurate as the SSD steps. We conclude that when substantial registration accuracy is required, the SSD refinement is still the best (albeit computationally expensive) alternative. The proposed ERPR method is a reasonable tradeoff for applications that require speed of computation. Specifically, for real-time vessel tracing, the ERPR algorithm only increases the computation time by 7.7% on average. Table 3 illustrates the impact of image rotation and scaling – the effects are clearly minimal.

VI. Discussion and Conclusions

The use of a specific model for vessel branch points and crossovers leads to more accurate and repeatable estimation of these locations and their signatures. Just a single iteration of the proposed algorithm leads to significant improvement in estimation accuracy.

Several line junction and corner detection techniques have been reported, including template matching [19, 20], gray-level dissimilarity measure [21], steerable filters [22], estimation of local line curvature [23, 24, 25], parametric model fitting [20] and parameterized feature detection by projecting local brightness distribution into the subspace [26]. Those techniques work either on gray-scale intensity by defining a junction as the point where two or more homogeneous surface patches are located within the neighborhood, or on curvature of the contour by extracting the junction as the point of local maximum change of gradient direction [27] estimates the density of nerve intersections by digitizing lines as row segments and deduce intersections from the adjacent overlapping segments. Our technique differs from others by extracting the junction as the closest point to the intersecting edges.

In addition to the intrinsic value in improved repeatability and reliability of landmark position estimation, there are several advantages to using ERPR. It's greatest value has been in the area of real-time spatial referencing, which is a much-improved alternative to image tracking. In this method, invariant feature vectors (indexes) are extracted from the landmark points, and used to

index into a database of pre-computed geometric invariants for the entire retina. The ERPR technique leads to significantly higher probability of successful registration on the first attempt, improving the reliability as well as the overall speed of referencing [7,28]. We anticipate similar benefits in other applications.

VII. Acknowledgments

Various portions of this research were supported by the National Science Foundation grant EIA-0000417, the Center for Subsurface Sensing and Imaging Systems, under the Engineering Research Centers Program of the National Science Foundation (Grant EEC-9986821), the National Institutes for Health grant RR14038, and by Rensselaer Polytechnic Institute. Thanks to Gary Howe and Mark Fish at the Center for Sight for retinal photography. Thanks to Dr. Ali Can at the Woods Hole Oceanographic Institute for valuable suggestions.

VIII. References

[1] Coatrieux, J. L., Garreau, M., Collorec, R., and Roux, C., "Computer Vision Approaches for the Three-Dimensional Reconstruction: Review and Prospects," Critical Rev. Biomed. Eng., 22(1):1-38, 1994.

[2] Robin, G. D., Paik, D. S., Johnston, P. C., and Napel, S., “Measurements of the Aorta and Its Branches with Helical CT, Radiology, Vol. 206, No. 3, pp. 823-829, 1999.

[3] Wilson, D. L., and Noble, J. A., “An Adaptive Segmentation Algorithm for Extracting Arteries and Aneurysms from Time-of-flight MRA data,” IEEE-TMI, Vol. 18, No. 10, pp. 938-945, Oct 1999.

[4] Can, A., H. Shen, J. N. Turner, H. L. Tanenbaum, and B. Roysam, "Rapid Automated Tracing And Feature Extraction From Live High-Resolution Retinal Fundus Images Using Direct Exploratory Algorithms," IEEE-TITB, vol. 3, no. 2, pp. 125-138, June 1999.

[5] Al-Kofahi, K., Lasek, S., Szarowski D., Pace, C., Nagy, G., Turner, J. N., Roysam, B., “Rapid Automated Three-dimensional Tracing of Neurons from Confocal Image Stacks,” IEEE-TITB, vol. 6, No. 2, June 2002.

[6] Wink, O., Niessen, W. J., Viergever, M. A., "Fast Delineation of Vessels in 3-D Angiographic Images," IEEE-TMI, vol. 19, No. 4, pp. 337-346, 2000.

[7] Shen, H., Roysam, B., Stewart, C. V., Turner, J. N., and Tanenbaum, H. L., "Optimal Scheduling of Tracing Computations for Real-time Vascular Landmark Extraction from Retinal Fundus Images," IEEE-TITB, vol.5, No. 1, March 2001.

[8] Goldbaum, M. H., Kouznetsova, V., Coté, B. L., Hart, W. E., and Nelson, M., "Automated Registration Of Digital Ocular Fundus Images For Comparison Of Lesions," in *SPIE: Ophthalmic Technologies III*, vol. 1877, 94-99, 1993.

[9] Saaristo, A., Karpanen, T., and Alitalo, K., "Mechanisms Of Angiogenesis And Their Use In The Inhibition Of Tumor Growth And Metastasis," *Oncogene*, 19(53):6122-9, Dec 2000.

[10] Kyriacos, S., Nekka, F., and Cartilier, L., "Insights into the Formation Process of the Retinal Vasculature", *Fractals*, Vol. 5, No. 4, pp. 615-624, 1997.

[11] Sequeira, J., Ebel, R., and Schmitt, F., "3-D Modeling of Tree-like Anatomical Structures," Computerized Medical Imaging and Graphics, vol. 17, no. 4/5, pp. 333-337, 1993.

[12] Schwartz, R. B., Jones, K. M., Chernoff, D. M., Mukherji, S. K., Khorasani, R., Tice, H. M., Kikinis, R., Hooton, S. M., Steig, P. E., and Polak, J. F., " Common Carotid Artery Bifurcation: Evaluation with Spiral CT," Radiology, Vol. 185, No. 2, pp. 513-519, 1992.

[13] Becker, D. E., Can, A., Tanenbaum, H. L., Turner, J. N., and Roysam, B. "Image Processing Algorithms For Retinal Montage Synthesis, Mapping, And Real-Time Location Determination," IEEE-TBME*,* 45(1), 1998.

[14] Tso, M. O. M, and Jampol, L. M. "Pathophysiology Of Hypertensive Retinopathy," Ophthalmologica 89:1132, 1982.

[15] Parida, L., Geiger, D., and Hummel. R., "Junctions: Detection, Classification, And Reconstruction," *IEEE-PAMI*, 20(7): 687-698, July 1998.

[16] Can, A., Stewart, C. V., Roysam, B., and Tanenbaum, H. L., "A Feature-Based Robust Hierarchical Algorithm for Registration Pairs of Images of the Curved Human Retina," IEEE-PAMI, vol. 24, no. 3, March 2002.

[17] Shen, H., Stewart, C. V., Roysam, B., Lin, G., and Tanenbaum, H. L., "Frame-Rate Spatial Referencing Based on Invariant Indexing and Alignment with Application to Laser Retinal Surgery," vol. 25, No. 3, IEEE-PAMI, March 2003.

[18] Brown, L.G., "A Survey of Image Registration Techniques," Surveys(24), No. 4, December 1992, pp. 325-376.

[19] Bigun, J., "A Structure Feature For Some Image Processing Application Based On Spiral Functions," *CVGIP*, 51:166-194, 1990.

[20] Rohr, K., "Recognizing Corners By Fitting Parametric Models," *International Journal of Computer Vision*, 9(3): 213-230, 1992.

[21] Cooper, J., Venkatesh, S., and Kitchen, L., "Early jump-out corner detectors," *IEEE-PAMI*, 15(8):823-829, Aug 1993.

[22] Simoncelli, E., and Farid, H., "Steerable Wedge Filters For Local Orientation Analysis," *IEEE Transactions on Image Processing*, 5(9): 1377-1383, 1996.

[23] Francois, D., and Djemel, Z., "Extracting Line Junctions From Curvilinear Structures," In *Proc. IEEE Geoscience and Remote Sensing Symposium,*vol. 4, pp. 1672-1674, 2000.

[24] Kitchen, L., and Rosenfeld, A., "Gray Level Corner Detection," *Pattern Recognition Letters*, (1): 95-102, Dec 1982.

[25] Mokhtarian, F., and Suomela, R., "Robust Image Corner Detection Through Curvature Scale Space," *IEEE-PAMI*, 20(12):1376-1382, Dec 1998.

[26] Nayar, S., Baker, S., and Murase, H., "Parametric Feature Detection," *Proceedings IEEE Conference on Computer Vision and Pattern Recognition*, pages 471-478, 1996.

[27] Sebok, T., Roemer, L., and G. Malindzak, Jr., "An Algorithm For Line Intersection Identification," *Pattern Recognition*, 13(2): 159-166, 1981.

[28] Lin, G., Fritzsche, K. L., Stewart, C. V., Tanenbaum, H. L., and Roysam, B., "Predictive Scheduling Algorithms for Real-time Feature Extraction and Spatial Referencing: Application to Retinal Image Sequences," (to appear) IEEE Trans. Biomedical Engr., April 2002.

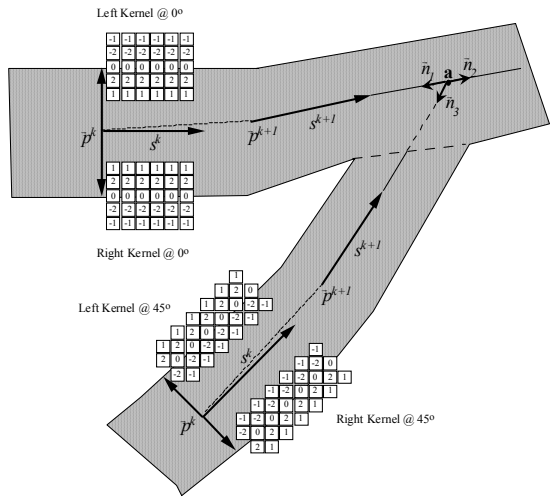

(a)

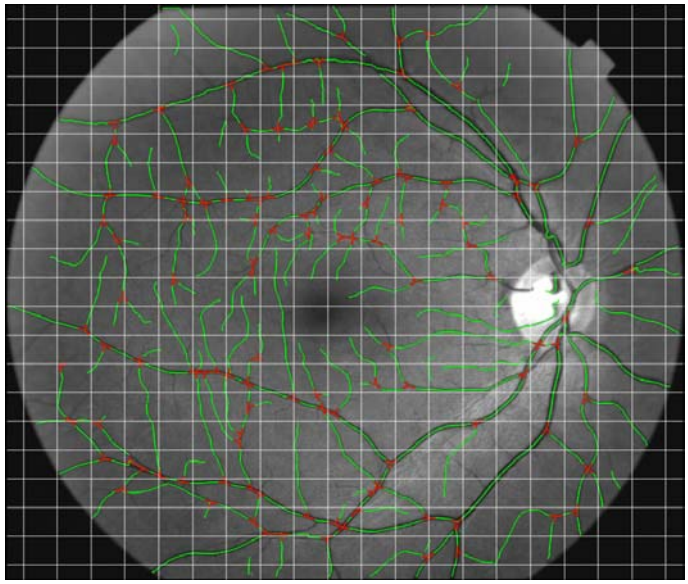

(b)

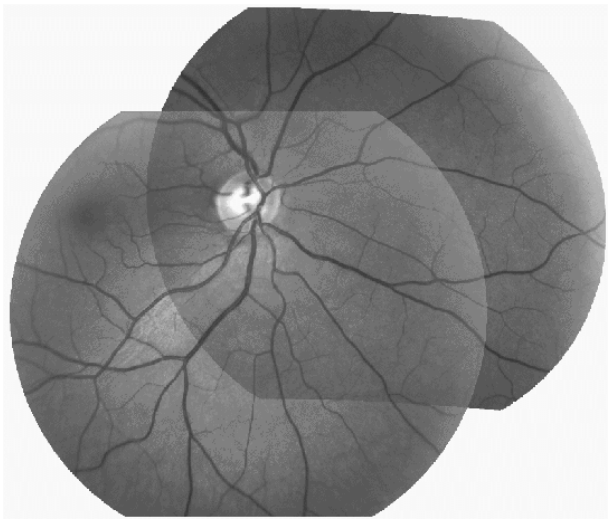

(c)

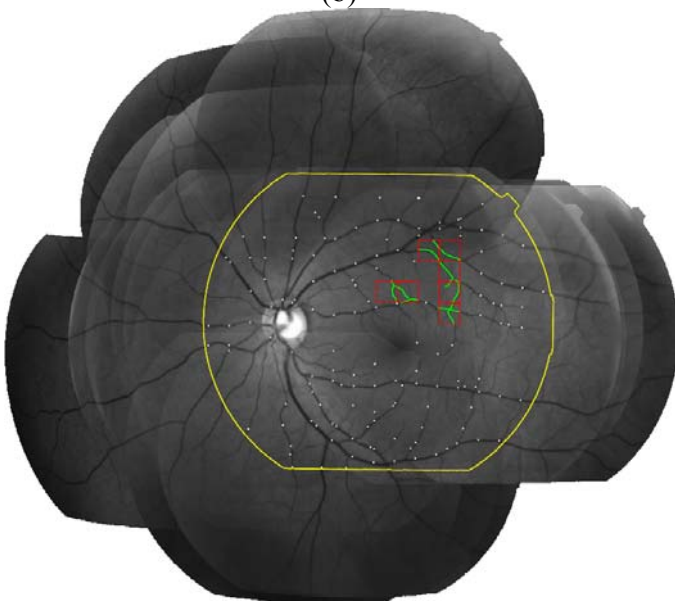

(d)

Figure 1: Examples from prior related work, illustrating fast tracing of branched structures. (a) Illustrating the recursive tracing algorithm based on a model that expects a pair of anti-parallel edges; (b) A fundus image, overlaid with results from the results from the exploratory tracing algorithm; (c) Registration of fundus images taken at the same time with approx. 50% overlap; (d) Illustrating spatial referencing with sparse feature extraction. Accurate registration to sub-pixel accuracy requires precise and repeatable estimation of image features (landmarks), and their signatures (intersection angles and thickness values).

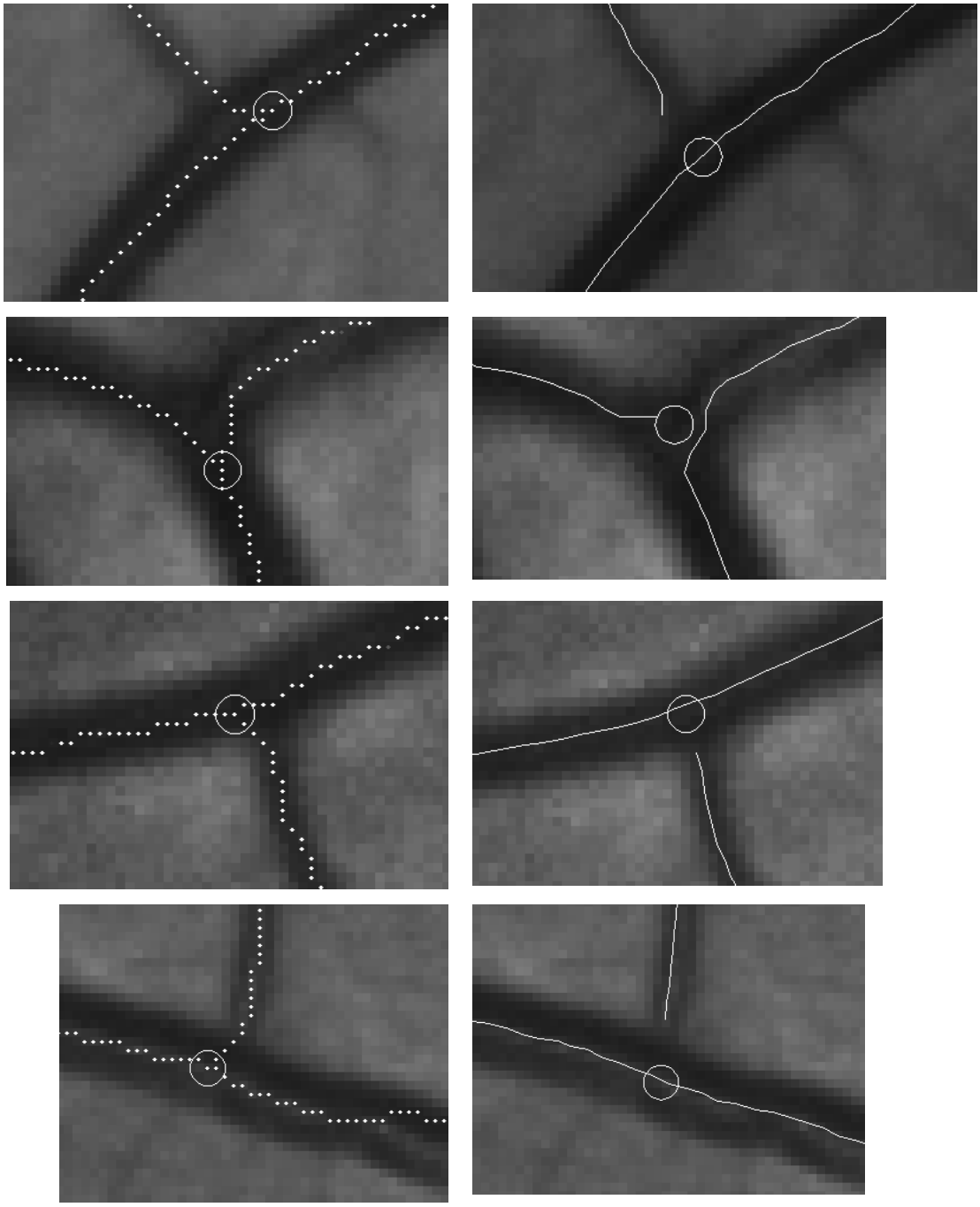

Figure 2: Illustrating the issue of landmark location accuracy. The left column shows enlarged close-up views of three landmarks, overlaid with the results of tracing from our earlier algorithm. As the tracing steps approach the intersection, the anti-parallel edges model that holds well for the straight portions of the vasculature fails, leading to errors in estimating the intersection position and angle. The column on the right shows results produced by the enhanced algorithm (ERPR) presented in this paper. This algorithm estimates the locations of the intersections, and the angular signatures more accurately using a model (illustrated in Figure 3). The detected intersection is the center of the overlaid circle.

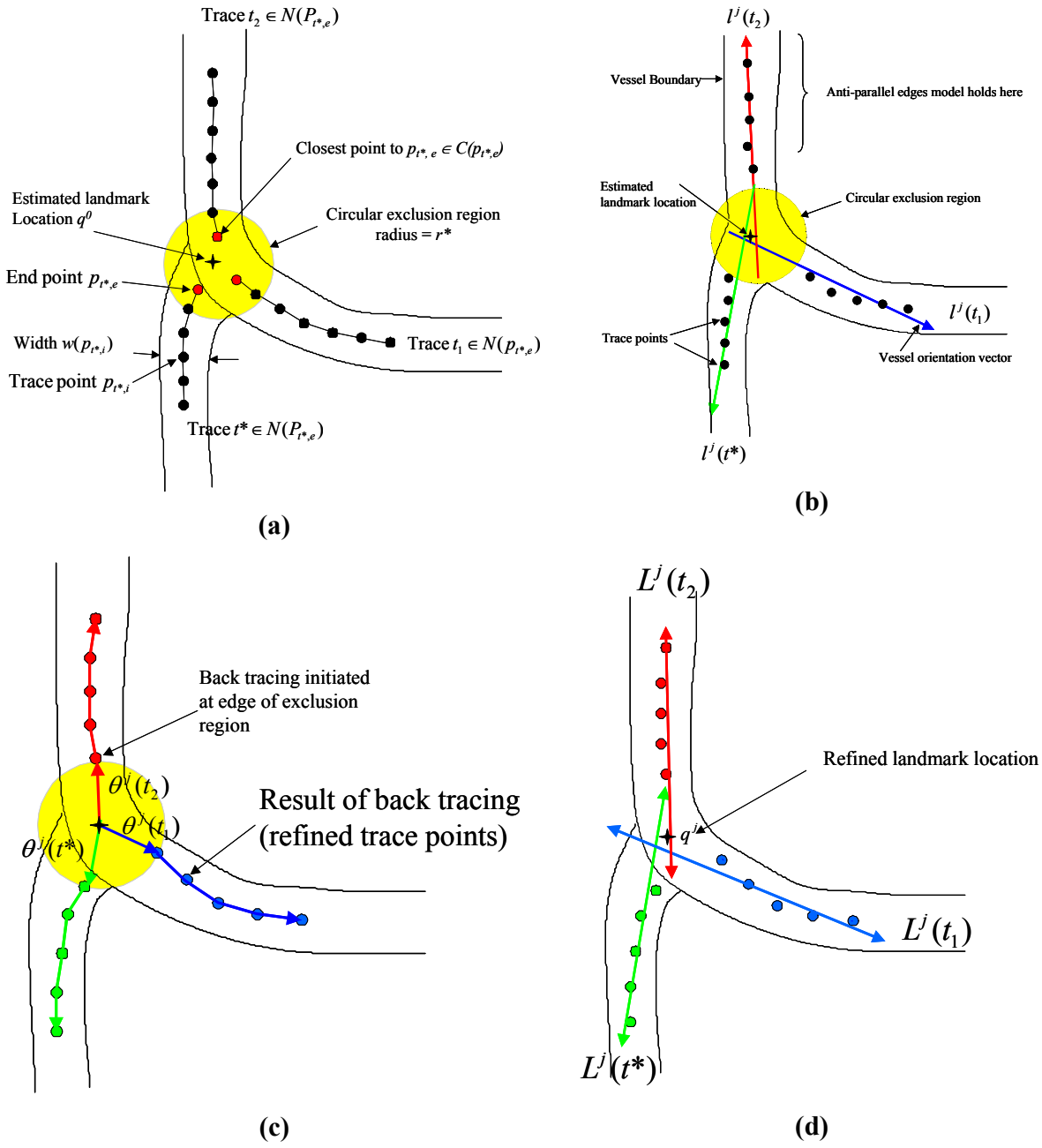

Figure 3: Illustrating the vessel intersection model and ERPR algorithm: (a) Notation and the result of initial tracing- the circular exclusion region (yellow) is the region over which the anti-parallel edges model for vessels is not valid, but the proposed model is. Traces farther away from the exclusion region provide estimates of the local vessel orientations. (b) Lines, $l^j(t_1)$, $l^j(t_2)$, and $l^j(t^*)$ are fit to the previously traced centerline points; (c) showing new traces from back-tracing, initiated from points that are estimated based on the angles of the fitted lines, and just outside the exclusion region; (d) The refined landmark location is estimated by fitting lines denoted $L^j(t_1)$, $L^j(t_2)$, and $L^j(t^*)$, and finding the point q^j that is closest to these lines.

Table 1: Landmark repeatability experiment. The original landmark method is compared to three versions of the new ERPR method: the full iterative refinement; the simplified version with one step of back trace refinement; and an even simpler version with no back trace refinement whatsoever.

	Location Distance		Max Orientation Difference	
	Median Error (Pixels)	Mean Error (Pixels)	Median Error (Degrees)	Mean Error (Degrees)
Original	2.09	2.21	7.20	8.63
ERPR, full	1.05	1.34	3.75	4.80
ERPR, simplified	1.07	1.33	4.33	5.43
ERPR, no back-trace	1.28	1.51	5.03	6.04

Table 2: Landmark position vs. SSD refined position: comparing the original landmark estimation technique to the new ERPR method with a just one step of back trace refinement.

	Location Error	
	Median (Pixels)	Mean(Pixels)
Original	2.04	1.76
ERPR, simplified	1.10	0.72

Table 3: Landmark repeatability under various rotation and scaling transformations:

	Location Error		Max Orientation Difference	
	Median (Pixels)	Mean (Deg)	Median (Pixels)	Mean (Deg)
Rotation	0.65	0.99	3.99	5.37
Different resolution	0.79	0.94	5.82	7.06
Same resolution	0.61	0.78	4.33	5.66

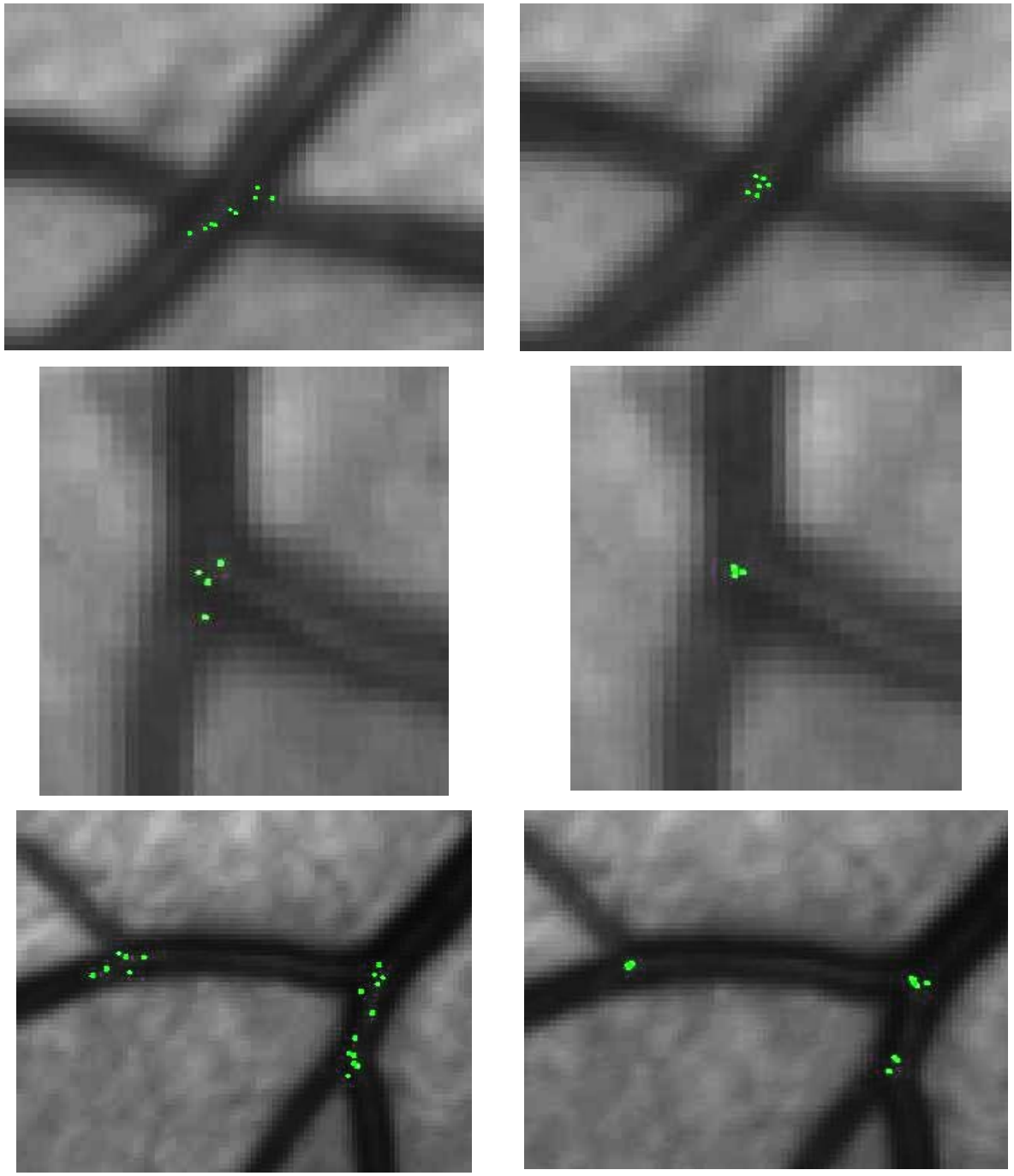

Figure 4: The green dots on the vessels are the landmarks mapped from the fundus images. The left column shows three examples from the original method. The right column shows the corresponding results from the ERPR algorithm for the same image regions. Observe the substantial improvement in the repeatability with which the locations are estimated. This is important for image registration applications, especially with real-time implementations.